PHYSICAL REVIEW B **95**, 220401(R) (2017)

Spin-polaron formation and magnetic state diagram in La-doped $CaMnO_3$

N. Bondarenko,[1] Y. Kvashnin,[1] J. Chico,[1] A. Bergman,[1] O. Eriksson,[1] and N. V. Skorodumova[1,2]
[1]*Division of Materials Theory, Department of Physics and Astronomy, Uppsala University, Box 516, 75121 Uppsala, Sweden*
[2]*Multiscale Materials Modelling, Department of Materials Science and Engineering, Royal Institute of Technology, SE-100 44 Stockholm, Sweden*

(Received 10 July 2016; published 7 June 2017)

$La_xCa_{1-x}MnO_3$ (LCMO) has been studied in the framework of density functional theory (DFT) using Hubbard-U correction. We show that the formation of spin polarons of different configurations is possible in the G-type antiferromagnetic phase. We also show that the spin-polaron (SP) solutions are stabilized due to an interplay of magnetic and lattice effects at lower La concentrations and mostly due to the lattice contribution at larger concentrations. Our results indicate that the development of SPs is unfavorable in the C- and A-type antiferromagnetic phases. The theoretically obtained magnetic state diagram is in good agreement with previously reported experimental results.

DOI: 10.1103/PhysRevB.95.220401

Perovskite $CaMnO_3$-$LaMnO_3$ (CMO-LMO) system exhibits an outstandingly rich magnetic and structural polymorphism [1]. $CaMnO_3$ (CMO) is an orthorhombic ($Pnma$) semiconductor with the band gap of 3.07 eV [2]. Its magnetic ground state is the G-type antiferromagnetic (G-AFM) structure, where each spin-up (down) atom is surrounded by six spin-down (up) atoms. Such a magnetic ordering is thought to be governed by the super-exchange interaction along the $Mn^{4+}(t_{2g}^3)\uparrow$-O($p$)-$Mn^{4+}(t_{2g}^3)\downarrow$ bond chains [3]. When trivalent La^{3+} substitute atoms in the Ca^{2+} sublattice extra valence electrons are added to the system. This extra charge can be redistributed among a large number of atoms or fully (partially) localized at the d orbitals of particular Mn atoms driving the double-exchange interaction in the mixed-valence $Mn^{3+}(e_g^1)\uparrow$-O(p)-$Mn^{4+}(t_{2g}^3)\uparrow$ bond alignment [4]. The Hund coupling may then assist the spin flip at the central site of the magnetic octahedron [5], thus forming a ferromagnetic (FM) seven-site droplet or the so-called seven-site spin polaron (SP). Such seven-site SPs can be joined together in different configurations forming larger FM droplets, for example, involving 12, 17, or 21 sites [6,7]. Unlike classical polarons, where an electron is trapped due to a strong electron-lattice interaction [8,9], spin polarons are thought to form largely due to magnetic interaction [10,11]. However, cooperative spin-charge-lattice effects are also important for SPs as the formation of the $Mn^{3+}(e_g^1)$ state leads to the symmetry breaking by Jan-Teller distortions becoming more pronounced as the number of Mn^{3+} atom increases. At a critical concentration the accumulated lattice deformation energy drives the magnetic transition to the C-type antiferromagnetic (C-AFM) state, which in La-doped $CaMnO_3$ is accompanied by the structural transition from $Pnma$ orthorhombic to the P_1/m monoclinic structure [1,6,12–14].

In Fig. 1 we summarize the available experimental data on the stability of the magnetic phases of $La_xCa_{1-x}MnO_3$ for $x_{La} < 0.2$. The concentrations at which the magnetic transitions are reported to take place vary depending on the experimental setups and applied methods, nonetheless, all the experiments clearly demonstrate the existence of four distinct regions (i)–(iv), described below.

(i) Concentration range $0 < x_{La} < 0.01$–0.03. For these small concentrations the G-AFM magnetic structure of CMO is preserved but the physical properties of the oxide are noticeably affected by doping. In particular, already 0.05–1% of La is enough to have a crucial impact on the Hall coefficient suggesting an increased mobility of charge carriers [15]. The measurements of electric conductivity confirm this suggestion reporting substantially higher values for the doped oxide compared to those for CMO [16,17]. The magnetic saturation curve, $M_s(x_{La})$, measured for LCMO with $x_{La} < 0.02$–0.03, shows a slope of only 1 μ_B/Mn, which is much smaller than should be expected in the case of a FM droplet forming in the G-AFM matrix [16,18]. This finding speaks in favor of a mean-field-like distribution of extra charge due to La doping rather than the electron localization scenario.

(ii) Concentration range 0.01–$0.03 < x_{La} < 0.06$–0.10. The oxide matrix still preserves the G-AFM order while a SP signature is also observed. The SP appearance has been detected by neutron powder diffraction, magnetization, Raman spectra, and the heat conductivity measurements [14,16,18–22]. In contrast to the measurements done for smaller concentrations [region (i)], the slope of the $M_s(x_{La})$ curve now increases to 8 μ_B/Mn [16,18], confirming SP presence. Interestingly, the measured spontaneous magnetization is significantly smaller than a value to be expected in the case of full electron localization that suggests a partial character of localization [21,23]. The neutron scattering measurements have distinguished isolated SPs of about 10.4 Å in size separated by 41 Å for $0.02 < x_{La} < 0.05$ and SPs up to 10.8 Å in size separated by 24 Å for $0.05 < x_{La} < 0.10$ [23,24].

(iii) Concentration range 0.06–$0.1 < x_{La} < 0.14$–0.18. Here one finds a complex mixture of magnetic structures including G-AFM with SPs and emerging C-AFM ordering, whose appearance is accompanied by the structural transition to the monoclinic (P_1/m) phase [14,16,18–23].

(iv) Concentration range 0.14–$0.18 < x_{La} < 0.2$. According to numerous experiments [14,16,18,20,21,23,24] the C-AFM monoclinic phase is the only observed phase in this concentration interval.

The pioneer *ab initio* calculation studying spin-polaron formation in La-doped CMO has shown that the charge localization at the SP sites has e_g character [12]. The study of the electron doped CMO, done employing model Hamiltonians, has demonstrated the stability of the seven-site SP solution

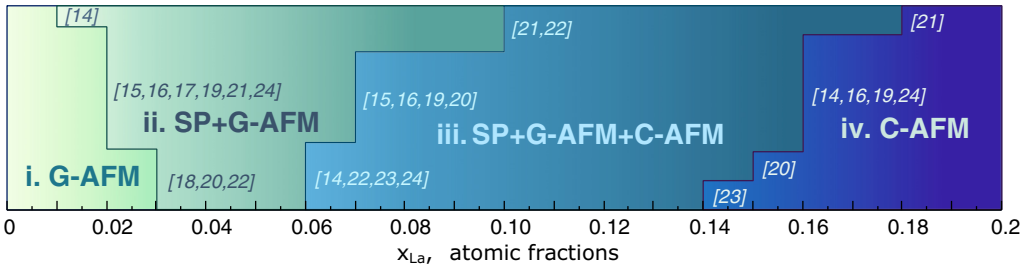

FIG. 1. LCMO magnetic state diagram in $0 < x_{La} < 0.20$ range according to the following experimental methods: neutron powder diffraction [14], magnetic properties [14–16,20,21], electrical conductivity [17], Raman scattering [19], thermal conductivity [18], electrical resistivity [20], specific heat capacity [22], and neutron scattering [23,24]. The phase diagram is divided into four segments: (i) G-AFM, (ii) FM droplets+G-AFM, (iii) FM droplets+G-AFM+C-AFM, (iv) C-AFM. See text for details.

[6,7,12]. The study of the model has also shown that beyond $x_{La} = 0.045$, seven-site SP becomes unstable with respect to a FM spin order [7].

Here we present a detailed *ab initio* description of the magnetic state diagram of $La_xCa_{1-x}MnO_3$ in the low-La concentration range. We consider the possibility for the SPs of different configurations to form in different AFM phases and analyze the role of magnetic and lattice contributions in their stabilization.

In our study we used the DFT+U approach, employing the projector augmented wave method [25] and the Perdew, Burke, Ernzerhof parametrization [26] of the exchange-correlation interaction as implemented in VASP [27]. The cutoff energy was 550 eV. The calculations were done for the 3×2×3 supercell containing 72 Ca, 72 Mn, and 216 O atoms. The La concentration was varied in the range of $0.013 < x_{La} < 0.133$ by replacing different number of Ca atoms by La (1–10 La/supercell). A 2×2×2 Monkhorst-Pack k-point mesh, which resulted in eight irreducible k points, was used for the integration over the Brillouin zone. In order to find the equilibrium orthorhombic ratio a structural optimization was performed at each x_{La} in the manner described in Ref. [28]. The lattice optimization was done keeping the G-AFM magnetic order. SPs were formed in the magnetic lattice by flipping the spin on the central atom in one or several Mn octahedra and allowing only atomic positions to relax. The presented here results were obtained in collinear spin calculations.

The choice of the Hubbard U parameter is always an important issue in the calculations of complex oxides. Here we estimated the effective U parameter ($U_{eff} = U - J$ [29]) using the linear response method developed by Cococcioni [30], which, depending on the choice of the basis set, resulted in $U_{eff}(Mn_{3d})$ in the range of 3.45–4.23 eV. For our calculations, however, we utilized the rotationally invariant approach [31]. This approach was shown to be more appropriate for the description of complex magnetic structures [32]. We used $J = 0.9$ eV, the most common value applied for this class of compounds [33]. Further, we varied U in the range of $U = 0.9$–8.9 eV that corresponds to $U - J = 0$–8 eV. We found that $U < 2.9$ eV overestimate the stability of the G-AFM structure, while $U > 4.9$ eV fail to describe the Mn_{3d}-O_{2p} hybridization and result in the stabilization of the long range FM structure. The U values between 2.9 and 4.9 eV reproduce qualitatively correct magnetic states, in agreement with experimental data [14,23,24] (Fig. 1). Based on the performed tests and the analysis of the parameters found in the literature [34–36], we chose to use $U = 3.9$ eV and $J = 0.9$ eV in the calculations presented here.

In Fig. 2 we show the density of states (DOS) obtained for the 7- and 21-sites SPs formed in G-AFM matrix for two La concentrations. The excess electrons, donated by La, occupy a shoulder near the Fermi level, which is hardly visible for $x_{La} = 0.013$ but becomes more evident as the La concentration increases (Fig. 2). This shoulder consists of the e_g states for all the studied SP configurations and La concentrations. The partial charge distribution shows that these e_g states are mostly localized at the SP sites and have $3z^2 - r^2, x^2 - y^2$ character. A somewhat larger degree of the Mn(e_g^1)-O(p) hybridization is observed in the (101) plane as compared to the others. We

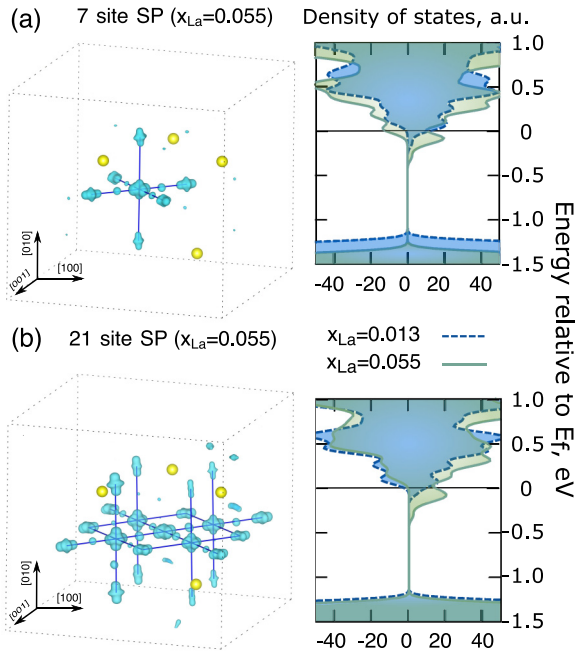

FIG. 2. (a) Charge distribution of e_g states (left panel) and the density of states (right panel) for seven-site SP for $x_{La} = 0.013$ and $x_{La} = 0.055$. (b) Charge distribution of e_g states (left panel) and the density of states (right panel) for 21-site SP for $x_{La} = 0.013$ and $x_{La} = 0.055$. In the charge distribution plots only the values in the energy range from −0.5 eV to the Fermi level are shown. The La atoms are shown in yellow.

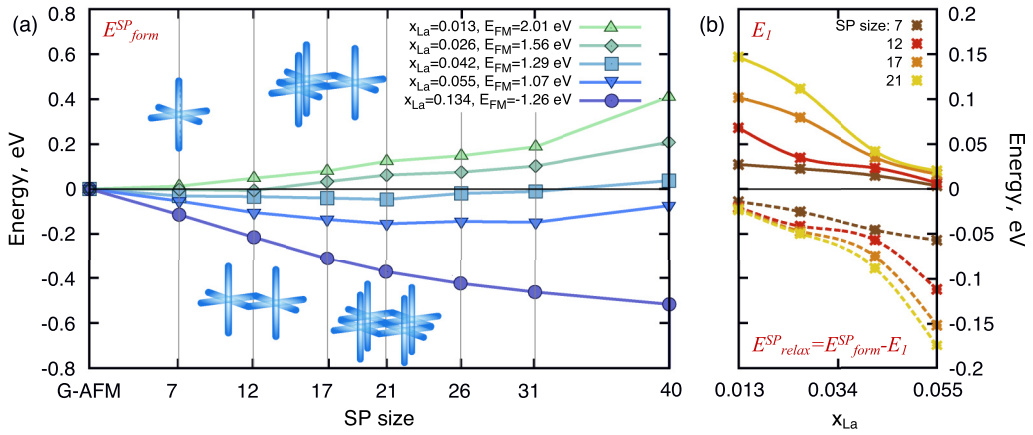

FIG. 3. (a) Total energies of spin polarons of various sizes formed in G-AFM as a function of La concentration. The SP energies are given with respect to that of G-AFM ($E^{\mathrm{SP}}_{\mathrm{form}}$). For illustration, 7-, 12-, 17-, and 21-site SPs are schematically shown. The energies of FM solutions (E_{FM}) are also listed in the legend for comparison. (b) Decomposition of $E^{\mathrm{SP}}_{\mathrm{form}}$ into the magnetic contribution (E_1, upper panel) and lattice relaxation contribution ($E^{\mathrm{SP}}_{\mathrm{relax}}$, lower panel). See text for details.

have also performed hybrid functional calculations (HSE06) [37,38] of the seven-site SP configuration and obtained very similar DOSs to the ones shown in Fig. 2.

We have checked the significance of the spin orbit coupling for the description of the magnetic structures in $La_xCa_{1-x}MnO_3$. We find that it additionally stabilizes SPs lowering their energy by about 10–15%.

The formation energies of different SPs in the G-AFM phase calculated for five La concentrations are presented in Fig. 3(a). For $x_{\mathrm{La}} = 0.013$ the G-AFM solution is more stable than the seven-site SP configuration by 13 meV. Larger SPs have higher energies and, therefore, even less stable with respect to G-AFM. However, already for $x_{\mathrm{La}} = 0.026$ the situation changes. At this concentration the 7 and 12-site SPs become preferable by 3 meV and 6 meV, respectively. As La concentration increases we observe further stabilization of spin polaron solutions. For $x_{\mathrm{La}} = 0.042$ and $x_{\mathrm{La}} = 0.055$ 21-site SP has the lowest energy, lower than that of G-AFM by 46 meV and 155 meV, respectively. This indicates a gradual development of a long range FM order, which we find to fully stabilize for the largest considered here concentration, $x_{\mathrm{La}} = 0.134$ (Fig. 3). Thus, we find the stabilization of the SP solutions between $x_{\mathrm{La}} = 0.026$ and 0.055. Most polaronic sites are situated in the (101) plane. The SPs prefer to form near the dopants. In particular, for $x_{\mathrm{La}} = 0.013$ we find that the energy of the seven-site SP increases by 18 meV as the SP-La separation distance changes from 3.34 Å to 6.56 Å.

Further, we analyze how the extra charge, brought into the system by La doping, is distributed in the oxide and how it affects local magnetic moments. If one considers the case of a full localization of an extra electron at the SP sites one would expect to find additional 1 μ_B per formed SP (or per La atom). The analysis of Bader charges, however, shows that for small La concentrations the extra charge is practically totally smeared over the atoms of the oxide matrix. For $x_{\mathrm{La}} = 0.013$ (1 La/supercell), for example, only 0.06 e^- for seven-site SP and 0.08 e^- for 21-site SP of additional charge are found at the polaronic sites as compared to the rest of the sites in the supercell. In this case the SPs show an additional magnetic moment of 0.57 μ_B/SP for seven-site SP and 0.47 μ_B/SP for 21-site SP. For $x_{\mathrm{La}} = 0.055$ (4 La/supercell) we find an extra 0.15 e^- (seven-site SP) and 0.20 e^- (21-site SP) with the additional magnetic moments of 1.49 μ_B/SP (seven-site SP) and 1.28 μ_B/SP (21-site SP). Therefore, we observe only partial charge localization at polaronic sites that agrees well with experimental findings [21,23].

To better understand the mechanism of the SP formation we try to separate lattice and magnetic contributions to the formation energy of the SP, $E^{\mathrm{SP}}_{\mathrm{form}}$, which is the difference between the total energies of the optimized supercell with SP and optimized G-AFM supercell. We estimate the contribution due to the spin subsystem reorganization by calculating the difference, E_1 [Fig. 3(b)], between the energy of the supercell where all the atoms are frozen in the positions corresponding to the optimized G-AFM structure but the spins are arranged as in SP, and the energy of the optimized G-AFM supercell. The difference between $E^{\mathrm{SP}}_{\mathrm{form}}$ and E_1 is the relaxation energy, $E^{\mathrm{SP}}_{\mathrm{relax}}$ [Fig. 3(b)], or the energy contribution due to structural rearrangements around SP [39]. Figure 3(b) demonstrates that the lattice relaxation for lower concentrations is rather small but it becomes substantially larger as La concentration increases. The positive magnetic contribution, on the contrary, decreases as more La is added. Therefore, the eventual stabilization of polarons is largely determined by the lattice contributions.

This conclusion is supported by the analysis of local lattice deformations. In particular, in the case of seven-site SP ($x_{\mathrm{La}} = 0.013$) the 6 Mn atoms surrounding the central Mn atom of SP shift away from it by ~5 mÅ and the surrounding oxygens move away by ~10 mÅ as compared to their positions in the G-AFM lattice. At the same time, Ca atoms come ~5 mÅ closer to the SP center. For higher La concentrations ($x_{\mathrm{La}} = 0.055$), the displacements increase to ~10 mÅ for Mn atoms, ~50 mÅ for O atoms, and ~20 mÅ for Ca atoms. At low concentrations mainly the atoms of the SP are displaced. For higher concentrations a majority of the atoms of the supercell become displaced and the distortion amplitude increases.

To clarify the total picture of the magnetic transitions in the low La concentration range we have examined four different magnetic phases experimentally observed in the CMO-LMO

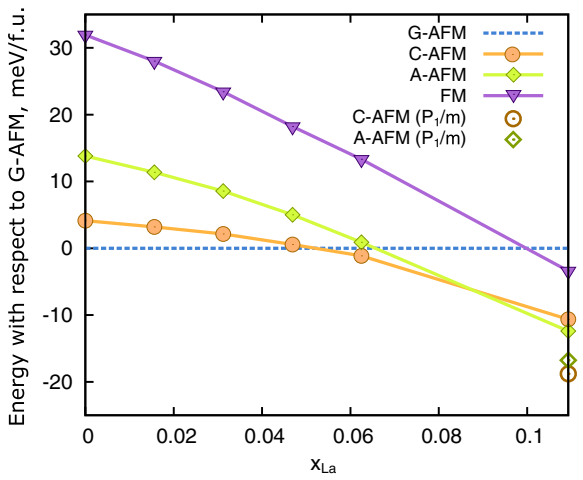

FIG. 4. Energies of different magnetic phases as a function of x_{La}. We show total energies per formula unit with respect to that of G-AFM.

system: G-AFM, C-AFM, A-AFM, and FM [40]. For these calculations we have preserved the equilibrium orthorhombic lattice parameters but optimized the atomic positions for each magnetic structure. The total energies of these phases with respect to the energy of the G-AFM phase are shown in Fig. 4. In the low concentration range, $0 < x_{La} < 0.052$, the G-AFM state is most stable. In concentration interval $0.052 < x_{La} < 0.091$ we see the stabilization of the C-AFM phase. Finally, for $0.091 < x_{La} < 0.103$ the A-AFM phase emerges. If we now compare data in Fig. 4 to those in Fig. 1 we will discover that the theoretically predicted stability intervals of G-AFM and C-AFM are in good agreement with the experimental observations. The stabilization of the A-AFM structure in the considered concentration range, however, does not agree with experiment (Fig. 1). As a matter of fact, this is the consequence of keeping the orthorhombic symmetry preserved. Indeed, allowing the symmetry of the supercell to optimize at $x_{La} = 0.11$ we find that it becomes monoclinic ($\beta = 0.91^\circ$, $a = 14.89$ Å, $b = 14.86$ Å, and $c = 15.12$ Å). The monoclinic C-AFM phase is 8 meV/f.u. lower in energy than the A-AFM orthorhombic structure and 2.1 meV/f.u. lower than the A-AFM monoclinic structure. Therefore, our results confirm the stabilization of the monoclinic C-AFM phase in this concentration range.

Additionally, we have checked the possibility for spin to flip and form some kind of local FM order in C-AFM and A-AFM phases. We notice that only the G-AFM structure naturally supports the appearance of FM droplets, which can be achieved by the flip of a single spin. The arrangements of spins in the C-AFM and A-AFM phases do not allow a local FM droplet to form by the same manipulation. Nevertheless we flipped one spin in each of the structures, relaxed the atomic positions, and compared the resulting total energies to that of the corresponding AFM structure. We found that the energies of all these configurations are higher than those of their parental AFM structures by 20–60 meV depending on La concentration.

To summarize, we propose an optimized approach, based on DFT+U, which allowed us to describe charge localization, spin polaron formation, and magnetic polymorphism of LCMO. We report the optimized geometries of SPs as a function of La concentration and provide a microscopic understanding of the relative importance of exchange and lattice effects for the formation of the spin polarons in La doped $CaMnO_3$.

N.V.S. acknowledges the financial support of the Swedish Research Council (VR) (project 2014-5993). O.E. acknowledges support from the Swedish Research Council (VR) and the Knut and Alice Wallenberg (KAW) foundation (Grants No. 2013.0020 and No. 2012.0031). We thank the Swedish National Infrastructure for Computing (SNIC) for providing computational resources.

[1] A. Moreo, S. Yunoki, and E. Dagotto, Science **283**, 2034 (1999).

[2] J. H. Jung, K. H. Kim, D. J. Eom, T. W. Noh, E. J. Choi, J. Yu, Y. S. Kwon, and Y. Chung, Phys. Rev. B **55**, 15489 (1997).

[3] H. A. Kramers, Physica **1**, 825 (1934); P. W. Anderson, Phys. Rev. **79**, 350 (1950); J. B. Goodenough, *ibid.* **100**, 564 (1955).

[4] C. Zener, Phys. Rev. **82**, 403 (1951); P. W. Anderson and H. Hasegawa, *ibid.* **100**, 675 (1955); P.-G. de Gennes, *ibid.* **118**, 141 (1960).

[5] C. Herring, in *Magnetism*, edited by J. Rado and H. Suhl (Academic Press, New York, 1965), Vol. 2.

[6] H. Meskine and S. Satpathy, J. Phys.: Condens. Matter **17**, 1889 (2005).

[7] Y. R. Chen and P. B. Allen, Phys. Rev. B **64**, 064401 (2001).

[8] N. Bondarenko, O. Eriksson, and N. V. Skorodumova, Phys. Rev. B **89**, 125118 (2014).

[9] S. Arapan, S. I. Simak, and N. V. Skorodumova, Phys. Rev. B **91**, 125108 (2015).

[10] D. R. Yakovlev and W. Ossau, Springer Ser. Mater. Sci. **144**, 221 (2010).

[11] D. Emin, *Polarons* (Cambridge University Press, Cambridge, 2013).

[12] H. Meskine, T. Saha-Dasgupta, and S. Satpathy, Phys. Rev. Lett. **92**, 056401 (2004).

[13] P. N. Santhosh, J. Goldberger, P. M. Woodward, T. Vogt, W. P. Lee, and A. J. Epstein, Phys. Rev. B **62**, 14928 (2000).

[14] C. D. Ling, E. Granado, J. J. Neumeier, J. W. Lynn, and D. N. Argyriou, Phys. Rev. B **68**, 134439 (2003).

[15] C. Chiorescu, J. J. Neumeier, and J. L. Cohn, Phys. Rev. B **73**, 014406 (2006).

[16] J. J. Neumeier and J. L. Cohn, Phys. Rev. B **61**, 14319 (2000).

[17] J. Lan, Y. Lin, A. Mei, C. Nan, Y. Liu, B. Zhang, and J. Li, J. Mater. Sci. Technol. **25**, 535 (2009).

[18] J. L. Cohn and J. J. Neumeier, Phys. Rev. B **66**, 100404(R) (2002).

[19] E. Granado, N. O. Moreno, H. Martinho, A. García, J. A. Sanjurjo, I. Torriani, C. Rettori, J. J. Neumeier, and S. B. Oseroff, Phys. Rev. Lett. **86**, 5385 (2001).

[20] R. Cortés-Gil, J. M. Alonso, J. M. Rojo, A. Hernando, M. Vallet-Regí, M. L. Ruiz-González, and J. M. González-Calbet, Chem. Mater. **20**, 3398 (2008).

[21] Y. Wang and H. J. Fan, Phys. Rev. B **83**, 224409 (2011).

[22] A. L. Cornelius, B. E. Light, and J. J. Neumeier, Phys. Rev. B **68**, 014403 (2003).

[23] E. Granado, C. D. Ling, J. J. Neumeier, J. W. Lynn, and D. N. Argyriou, Phys. Rev. B **68**, 134440 (2003).

[24] C. D. Ling, E. Granado, J. J. Neumeier, J. W. Lynn, and D. N. Argyriou, J. Magn. Magn. Mater. **272–276**, 246 (2004).

[25] P. E. Blöchl, Phys. Rev. B **50**, 17953 (1994); G. Kresse and D. Joubert, *ibid.* **59**, 1758 (1999).

[26] J. P. Perdew, K. Burke, and M. Ernzerhof, Phys. Rev. Lett. **77**, 3865 (1996).

[27] G. Kresse and J. Hafner, Phys. Rev. B **47**, 558(R) (1993); **49**, 14251 (1994); G. Kresse and J. Furthmuler, Comput. Mater. Sci. **6**, 15 (1996); Phys. Rev. B **54**, 11169 (1996).

[28] N. Bondarenko, O. Eriksson, and N. V. Skorodumova, Phys. Rev. B **92**, 165119 (2015).

[29] S. L. Dudarev, G. A. Botton, S. Y. Savrasov, C. J. Humphreys, and A. P. Sutton, Phys. Rev. B **57**, 1505 (1998).

[30] M. Cococcioni and S. de Gironcoli, Phys. Rev. B **71**, 035105 (2005).

[31] A. I. Liechtenstein, V. I. Anisimov, and J. Zaanen, Phys. Rev. B **52**, R5467(R) (1995).

[32] B. Himmetoglu, A. Floris, S. de Gironcoli, and M. Cococcioni, Int. J. Quantum Chem. **114**, 14 (2014).

[33] V. I. Anisimov, J. Zaanen, and O. K. Andersen, Phys. Rev. B **44**, 943 (1991).

[34] Z. Popović and S. Satpathy, Phys. Rev. Lett. **88**, 197201 (2002).

[35] J. Hong, A. Stroppa, J. Íñiguez, S. Picozzi, and D. Vanderbilt, Phys. Rev. B **85**, 054417 (2012).

[36] U. Aschauer, R. Pfenninger, S. M. Selbach, T. Grande, and N. A. Spaldin, Phys. Rev. B **88**, 054111 (2013).

[37] J. Heyd, G. E. Scuseria, and M. Ernzerhof, J. Chem. Phys. **118**, 8207 (2003); J. Heyd and G. E. Scuseria, *ibid.* **120**, 7274 (2004).

[38] The test calculations with hybrid functional were performed for a smaller unit cell (1 La, 15 Ca, 16 Mn, and 48 O atoms).

[39] The contributions vary with the SP size being much larger for 17- and 21-site configurations than for 7-site and 12-site SPs. If the curves are normalized by the corresponding number of sites in each polaron they become much closer to each other but show the same general trend. We also note that the total energy calculated for each La concentration would slightly depend on La and polaron distributions in the supercell. Our tests show that the energy variation can be up to 10–15 meV/La.

[40] E. O. Wollan and W. C. Koehler, Phys. Rev. **100**, 545 (1955).